PHYSICAL REVIEW D VOLUME 23, NUMBER 12 15 JUNE 1981

Fluctuating string of lattice gauge theory: The heavy-quark potential, the restoration of rotational symmetry, and roughening

J. B. Kogut and D. K. Sinclair
Physics Department, University of Illinois, Urbana, Illinois 61801

R. B. Pearson and J. L. Richardson
Institute for Theoretical Physics, Santa Barbara, California 93106

J. Shigemitsu
Physics Department, Brown University, Providence, Rhode Island 02912

(Received 30 January 1981)

String dynamics, the heavy-quark potential, and the restoration of rotational symmetry in lattice gauge theory are studied using Hamiltonian methods. We find that off-axis strings experience unbounded transverse fluctuations at all finite couplings. A fermion formulation of lattice strings is used to do systematic calculations. The heavy-quark potential is seen to have power-law corrections to linear confinement. Rotational symmetry in the string sector of the theory is restored in two stages. There is a finite coupling g_R ("roughening") where the equipotential surfaces of the heavy-quark potential become well-approximated by spheres, and there is the bulk critical point $g = 0$ where short-distance violations of rotational symmetry disappear. A new order parameter, the "kink" mass, is introduced to distinguish the smooth and rough phases of the string sector of any lattice gauge theory. Roughening coupling constants are determined using the kink mass for a variety of theories. These results are compared against more traditional width calculations. In the Hamiltonian formulation of SU(3) lattice gauge theory the roughening point lies inside the weak-coupling region.

I. INTRODUCTION

Lattice formulations of gauge theories are proving to be effective tools for studying strong interactions. Systematic studies using strong-coupling[1] and Monte Carlo[2] simulations have generated numerical evidence for quark confinement in pure non-Abelian gauge theories in 3+1 dimensions. A simple physical picture of confinement accompanies these numerical results. Familiar arguments show that the lattice theory confines quarks at strong coupling because of an "electric Meissner effect"—the ground state repels chromoelectric flux forcing the flux existing between a widely separated quark and antiquark into a tube of finite intrinsic width.[3] The numerical studies have shown that as the lattice coupling is decreased the properties of the theory smoothly approach those expected from ordinary weak-coupling perturbation theory.[1,2] This is good evidence for the fact that the properties of the lattice disappear in the continuum limit, Lorentz invariance is restored, and confinement remains.

These successes have led us to study the dynamics of flux tubes ("strings") in more detail. We are particularly interested in understanding the heavy-quark potential for all distances $\vec{r}$ and the restoration of rotational symmetry in the string sector of the theory. This work has led us to the following ideas.

(1) The static-flux-tube picture of confinement is incomplete. In a renormalized, continuum limit the flux tube experiences unbounded transverse fluctuations.

(2) The heavy-quark potential contains terms in addition to linear confinement. If $|\vec{r}|$ is much greater than the bulk correlation length (reciprocal of the glueball mass), then $V(\vec{r})$ has an asymptotic expansion,

$$V(\vec{r}) = T|\vec{r}| + \frac{\alpha_1}{|\vec{r}|} + \frac{\alpha_2}{|\vec{r}|^2} + \cdots \tag{1.1}$$

and the constants α_i are computable by lattice techniques.

(3) The restoration of rotational symmetry occurs in two steps in the string sector of the theory. There is a finite coupling g_R ("roughening") where the equipotential surfaces of the heavy-quark potential are well approximated by spheres. Short-distance violations of rotational symmetry disappear at the bulk critical point $g = 0$.

It is interesting to briefly consider the physics behind these three observations. Consider a flux tube placed along a coordinate axis of a spatial lattice. At strong coupling, where electric energy dominates the lattice Hamiltonian, distortions of the straight flux tube cost finite amounts of energy. Therefore, the string is essentially straight ("smooth"). The crucial question is whether the string remains smooth in the continuum limit of the lattice model. The answer is "no" and the

reason lies in simple considerations. The lattice theory itself possesses only discrete elements of the translation and rotation groups of a space-time continuum. At a strong-coupling, long-wave length, gradual fluctuations of the string are absent because of the lattice scaffolding. Thus, the on-axis lattice string has a qualitatively different excitation spectrum than its continuum partner. Elementary considerations show that a string in a space-time continuum can support fluctuations of arbitrarily long wave lengths and low energies. Of course, as the lattice coupling g is decreased one expects the on-axis string to evolve into its continuum relative. It is clear, however, that it cannot do this in an analytic fashion because the two strings have qualitatively different excitation spectra. In fact, several investigations have shown that the lattice string experiences a phase transition called roughening at a *finite* coupling g_R where it develops many properties of the more familiar physical continuum string.[4] At all couplings between g_R and the bulk critical point $g=0$, the lattice string experiences unbounded transverse fluctuations because its excitation spectrum has no mass gap.

The fact that $g_R \neq 0$ presents a serious challenge to lattice calculations. The nonanalyticity in the string tension at g_R limits the use of strong-coupling expansions. The unbounded transverse fluctuations make computer simulations on small lattices subject to systematic error. One needs a lattice approach to string dynamics which properly incorporates unbounded transverse fluctuations. Nontrivial, useful steps towards this goal are presented in this paper. We have found it useful to consider the *off-axis* string. Place a quark and an antiquark at arbitrary positions on a spatial lattice. Then even at strong coupling the string between them does not travel a unique path—any path of equal length contributes to the state of the string. Therefore, to study strings at a general orientation with respect to the lattice and, equivalently, the spatial character of the interquark potential, one must first solve a nontrivial problem in degenerate perturbation theory. This will be developed in detail in the next section of this article. We shall find that the off-axis, fluctuating string is "rough" for all finite coupling g. The fluctuating string will be described by fermion variables. In addition, a straightforward calculation reveals that the transverse fluctuations of the string are unbounded—strings with nonzero tension and length L experience transverse fluctuations of mean width $\ln L$ in $2+1$ dimensions.

The second observation listed above is closely related to the first. The energy in the fluctuating-string sector of the theory is the adiabatic potential between heavy quarks. The absence of a mass gap in the spectrum of the fluctuating string induces corrections to linear confinement which are power behaved in $|\vec{r}|$. The very existence of massless modes on the string generates the $\alpha_1/|\vec{r}|$ term of Eq. (1.1) and the coefficient α_1 is believed to be universal—independent of the gauge group.[5] Strong-coupling expansions for T and the α_1 coefficients can be developed using lattice perturbation theory and some relatively short series are presented here.

One of the virtues of the lattice approach is that $V(\vec{r})$ can be studied for all $|\vec{r}|$—large or small compared to the bulk correlation length. Formulas more general than the asymptotic expansion Eq. (1.1) will be presented in the text. In addition, the restoration of rotational symmetry can now be studied in a systematic fashion. At strong coupling the flux between the quark and antiquark must travel along a path of minimal length. So,

$$V(\vec{r}) = \frac{g_0^2}{2a}\frac{4}{3}(|x|+|y|+|z|), \quad g_0^2 \gg 1 \qquad (1.2)$$

where g_0 is the bare coupling on a spatial lattice of spacing a. The equipotential surfaces of Eq. (1.2) are octahedrons. In a proper continuum limit the equipotential surfaces must be spheres. As g_0 decreases and Eq. (1.2) is modified by finite coupling corrections, the octahedrons must evolve into spheres. But the octahedrons are not differentiable surfaces—they have kinks along each coordinate axis. Therefore, the octahedrons cannot evolve into spheres in an analytic fashion. In fact, we shall see in the text that the kinks in the octahedrons disappear at the roughening point g_R and the equipotential surfaces are well approximated by spheres for all $g \leq g_R$. Thus, rotational symmetry is restored in two stages in the string sector—at g_R where the equipotentials become spheres and at $g=0$ where short-distance asymmetries of the more familiar kind are washed out.

It should be clear to the reader that our investigations cast the roughening transitions of lattice gauge theory in a fresh light. We study roughening for several models in $2+1$ and $3+1$ dimensions by studying the mass spectrum of the on-axis string directly. We are led by our various considerations to consider the "kink" state of a string. This is a configuration of flux with one transverse link on an otherwise straight on-axis configuration. Roughening occurs at that coupling where the energy difference between this configuration and the straight string vanishes. Using the kink mass as the order parameter distinguishing the smooth string phase from the rough string phase, we locate the roughening coupling for Hamiltonian

SU(3) lattice gauge theory. g_R is seen to lie in the weak-coupling region, i.e., at a coupling distinctly smaller than that characterizing the rapid crossover from weak to strong coupling in the theory. This result should be contrasted with recent determinations of g_R in the Euclidean four-dimensional versions of SU(2) and SU(3) lattice gauge theory.[6] There g_R was found to lie in the middle of the crossover region. The Hamiltonian regularization procedure is, therefore, better suited to studying string dynamics and confinement. And certainly strings themselves and heavy quark potentials are better analyzed in a Hamiltonian (or transfer matrix) formalism.

In the final section of this article traditional width calculations are presented to determine g_R. They are in good agreement with the kink calculation conclusions.

II. THE SPATIAL STRUCTURE OF THE QUARK-ANTIQUARK POTENTIAL AND THE FLUCTUATING QUANTUM CHROMODYNAMICS (QCD) STRING

In this section we shall discuss the strong-coupling limit of the static quark-antiquark potential as a function of the separation vector $\vec{x}=(x,y,z)$. We will find that when the separation vector is *not* directed along a lattice axis, a wealth of new physics emerges. By looking away from the coordinate axes we will see that the string or flux tube connecting the $q\bar{q}$ pair will wander without bound as their separation distance is increased. In fact, we will find that the width of this flux tube will diverge logarithmically with the separation distance of the $q\bar{q}$ pair. These soft transverse string fluctuations will be responsible for inverse-power-law corrections to the pure linear confining potential. As the coupling is weakened we shall find that the $q\bar{q}$ potential tends to a rotationally invariant form as it must in order to have a sensible continuum limit.

Consider a static quark-antiquark pair located at the origin $(0,0,0)$ and at the point $\vec{x}=(x,y,z)=a(n_x,n_y,n_z)$ on a regular cubic lattice with lattice spacing a. The physics is described by the lattice gauge theory Hamiltonian[3]

$$H=\frac{g_0^2}{2a}\left[\sum_l E_l^2-\frac{2}{g_0^4}\sum_p \mathrm{tr}(U_p+U_p^\dagger)\right], \tag{2.1}$$

where a is the lattice spacing and g_0 is the bare coupling constant. The sums extend over the links l and the simple plaquettes p of the regular cubic lattice. E^2 is the quadratic Casimir operator on links and U_p is the group element in the fundamental representation of SU(3) obtained from the oriented product of group elements around plaquette p.

We would like to compute the energy of a state with a $q\bar{q}$ pair present, relative to the vacuum energy, as a power-series expansion in the strong-coupling expansion parameter $x_s=2/g_0^4$. Such a series may clearly be written in the form

$$V(x,y,z)=\frac{g_0^2}{2a}\sum_{n=0}^{\infty}(x_s)^n V_n(n_x,n_y,n_z)\,. \tag{2.2}$$

In states which contain quarks, electric flux conservation requires that there be one unit of electric flux flowing between the quark and the antiquark.[3] The lowest-energy states in the strong-coupling limit $x_s\to 0$ are those with each of the links on the shortest of paths joining the $q\bar{q}$ pair in the fundamental representation, and all others in the singlet representation. Such a state is shown in Fig. 1 and the energy of such a state is given to zeroth order in x_s by

$$V(x,y,z)=\frac{g_0^2}{2a}\frac{4}{3}(|n_x|+|n_y|+|n_z|)$$
$$=\frac{g_0^2}{2a}V_0(n_x,n_y,n_z)\,. \tag{2.3}$$

The equipotential surfaces of this zeroth-order potential are octahedrons which are clearly non-analytic along the coordinate axes as can be seen in Fig. 2. The set of all such paths with this same energy value are those with n_x steps along the x axis, n_y steps along the y axis, and n_z steps along the z axis taken in any order. The number of degenerate paths is thus

$$\frac{(|n_x|+|n_y|+|n_z|)!}{|n_x|!\,|n_y|!\,|n_z|!}\,. \tag{2.4}$$

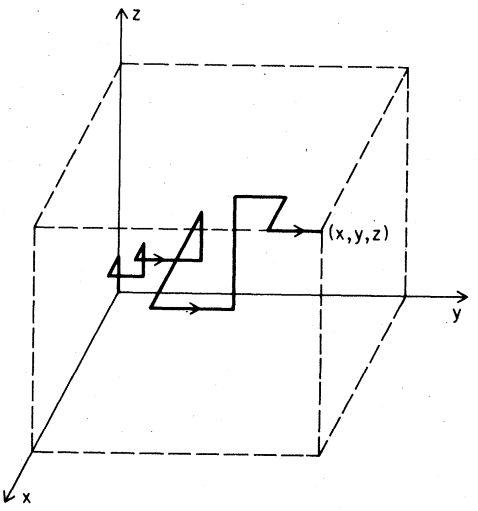

FIG. 1. A typical string state connecting a static $q\bar{q}$ pair.

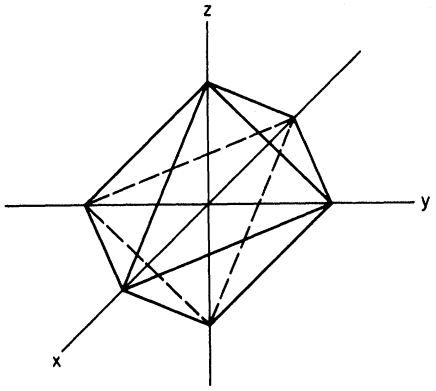

FIG. 2. The zeroth-order equipotential surface. Note the nonanalyticities along the coordinate axes.

To first order in x_s, all of these degenerate states are mixed by the second term in Eq. (2.1) and these terms are shown in Fig. 3. The potential exchanges nearest-neighbor link pairs which are not parallel. To compute the first-order energy shift $V_1(n_x, n_y, n_z)$, we must diagonalize the perturbation in the subspace of degenerate zeroth-order states. The formalism for diagonalizing the mixing matrix was discussed at great length in Ref. 7, where it was found that an exact diagonalization could be performed for arbitrary n_x and n_y in the plane $n_z = 0$. We shall now restrict ourselves to this case and study $V(x,y) \equiv V(x,y,0)$ and return later to the general case.

As was shown in Ref. 7, to first order in $x_s = 2/g_0^4$ the Hamiltonian of the system when $z = 0$ is equivalent to a system of $|n_y|$ fermions confined to a box of length $L = |n_x| + |n_y|$. There it was shown that the first-order effective Hamiltonian is given by

$$\frac{2a}{g_0^2} H_{\text{eff}} = \frac{4}{3} L - \frac{x_s}{3} \sum_{i=1}^{L-1} (a_i^\dagger a_{i+1} + a_{i+1}^\dagger a_i) , \tag{2.5}$$

which acts in the subspace of $|n_y|$ particles created by the fermion operator $a^\dagger$'s. These fermions represent electric flux in the y direction and the vacancies or empty sites represent flux in the x direction. The hopping term in (2.5) is responsible for exchanging an xy link pair with a yx pair as was shown earlier in Fig. 3. This Hamiltonian is diagonalized by introducing the single-particle wave functions

$$\phi_n(i) = \left(\frac{2}{L+1}\right)^{1/2} \sin\left(\frac{\pi n i}{L+1}\right), \quad n = 1, 2, \ldots, L \tag{2.6}$$

and fermion operators

$$b_n = \sum_{i=1}^{L-1} \phi_n(i) a_i , \qquad n = 1, 2, \ldots, L$$
$$b_n^\dagger = \sum_{i=1}^{L-1} \phi_n(i) a_i^\dagger . \tag{2.7}$$

With these substitutions, one easily finds that

$$\frac{2a}{g_0^2} H_{\text{eff}} = \frac{4}{3} L - \frac{x_s}{3} \sum_{n=1}^{L} \epsilon_n b_n^\dagger b_n \tag{2.8}$$

with a free single-particle spectrum given by $\epsilon_n = 2\cos[\pi n/(L+1)]$. In the string sector of the theory there are $|n_y|$ particles present and the lowest-energy state is the one with the first $|n_y|$ levels occupied, i.e., a filled "Fermi sea." The energy is then given by

$$\frac{2a}{g_0^2} V(x,y) = \tfrac{4}{3} L - \frac{x_s}{3} \sum_{n=1}^{|n_y|} 2\cos\left(\frac{\pi n}{L+1}\right)$$
$$= \tfrac{4}{3}(|n_x| + |n_y|) - \frac{x_s}{3} \frac{\cos\left(\frac{\pi}{2} \frac{|n_x| - |n_y|}{|n_x| + |n_y| + 1}\right)}{\sin\left(\frac{\pi}{2(|n_x| + |n_y| + 1)}\right)} . \tag{2.9}$$

Before we go on to compute the higher-order correction to this low-order result, there are many questions to ask of this simple first-order one. First, we ask about the angular and radial dependence of the $q\bar{q}$ energy. To display this dependence, we rewrite Eq. (2.8) in dimensionless polar coordinates r and θ where $n_x = r\cos\theta$ and $n_y = r\sin\theta$. We see that

$$\frac{2a}{g_0^2} V(r,\theta) = \tfrac{4}{3} r(|\cos\theta| + |\sin\theta|) - \frac{x_s}{3}\left[\frac{\cos\left(\frac{\pi}{2} \frac{|\cos\theta| - |\sin\theta|}{|\cos\theta| + |\sin\theta| + 1/r}\right)}{\sin\left(\frac{\pi}{2r} \frac{1}{(|\cos\theta| + |\sin\theta| + 1/r)}\right)} - 1\right] . \tag{2.10}$$

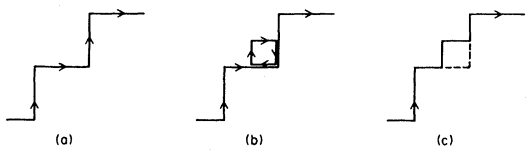

FIG. 3. The mixing term. The potential has the effect of exchanging link pairs which are different. (a) Initial-string state; (b) string state and potential term; (c) final-string state.

The angular dependence of Eq. (2.9) is most easily displayed by plotting the equipotential surfaces $V(r,\theta)=$ constant. These surfaces are shown in Fig. 4 for several values of x_s. We see from the figure that as x_s is increased from zero that the surfaces evolve continuously from squares into almost perfect circles when $x_s \simeq 2$. As x_s is increased beyond this value this circularity is lost, but one hardly expects such a low-order result to be valid for such large values of x_s. One actually expects this circularity to persist as $x_s \to \infty$ so that the weak-coupling theory is rotationally invariant.

To display the radial dependence of our result it is convenient to expand $V(r,\theta)$ in the form

$$V(r,\theta)=\frac{g_0^2}{2a}\sum_{l=-1}^{\infty} r^{-l} f_l(\theta, x_s) \tag{2.11}$$

and of course each of the f_l's may be separately expanded in x_s. Of particular interest is the angular-dependent tension $f_{-1}(\theta, x_s)$ which we obtain to first order in x_s by expanding Eq. (2.9),

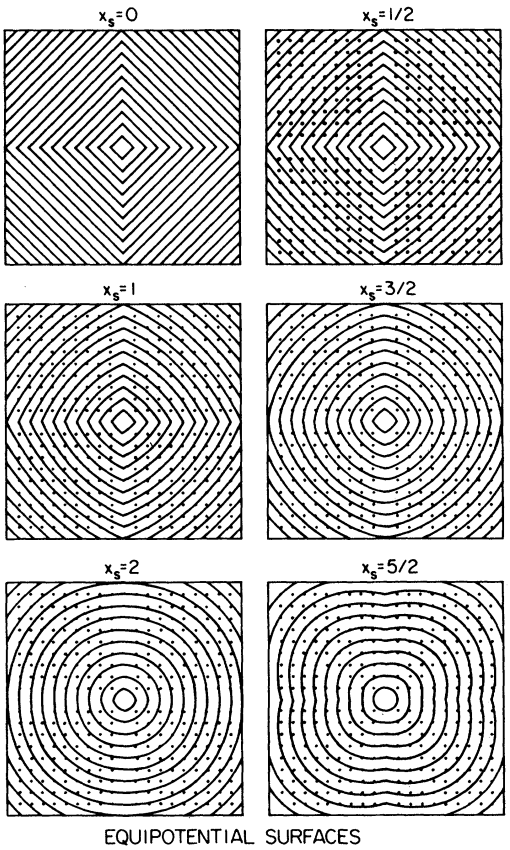

FIG. 4. The first-order equipotential surfaces for various values of x_s. The small dots denote lattice sites.

$$f_{-1}(\theta, x_s)=\tfrac{4}{3}(|\cos\theta|+|\sin\theta|)\left[1-\frac{x_s}{2\pi}\sin\left(\frac{\pi}{1+|\tan\theta|}\right)\right]. \tag{2.12}$$

When $x_s=2$ this function is almost independent of θ and differs from a constant by a maximum relative error of 2 percent.

We also examine the "Coulomb term" $f_1(\theta, x_s)$ in Eq. (2.10) to see whether it is attractive or repulsive. We find that

$$f_1(\theta, x_s)=-x_s\frac{\pi}{18}\frac{(4|\sin\theta||\cos\theta|-1)}{(|\sin\theta|+|\cos\theta|)^3}\sin\left(\frac{\pi}{1+|\tan\theta|}\right) \tag{2.13}$$

which can have either sign, depending on θ. $f_1(\theta, x_s)$ is mostly negative, however, for if we average over all angles we find $-0.022x_s$, which suggests that the Coulomb term is indeed attractive.

Another extremely interesting quantity to measure in our first-order QCD string is the "width" of the string. For simplicity consider a string at 45° when $n_x=n_y$. For such a string we would like to compute its width at the string's center. To calculate it, we will need an operator which measures the string's perpendicular coordinate $x_\perp$ at the string's center. A little thought shows that such an operator is given by

$$x_\perp=\frac{1}{\sqrt{2}}\left(\sum_{l=1}^{L/2} a_l^\dagger a_l-\sum_{l=L/2+1}^{L} a_l^\dagger a_l\right). \tag{2.14}$$

$x_\perp$ simply counts the differences between the number of particles in the left and right halves of the box. Several string states and their associated $x_\perp$'s are demonstrated in Fig. 5. We would like to know how the string's mean-square width $x_\perp^2$ behaves as the string's length L is increased. By expressing Eq. (2.14) in terms of the single-particle operators and wave functions of Eqs. (2.5) and (2.6) one finds that in the string's lowest-energy state,

$$\langle x_\perp^2\rangle \sim \ln L \tag{2.15}$$

for L large. This result says that the electric flux is *not* confined to a region of finite width as the $q\bar{q}$ pair's separation distance is increased. This logarithmic behavior is reminiscent of the continuum-string-model result.[5]

Still restricting our discussion to the plane $z=0$, we now look at the higher-order corrections to our first-order result. To second order in x_s, there are five district graphs that contribute to $V(x,y)$ which are displayed in Fig. 6. As can be seen in the figure, three of the graphs are diagonal and two are off diagonal. The SU(3) group weights

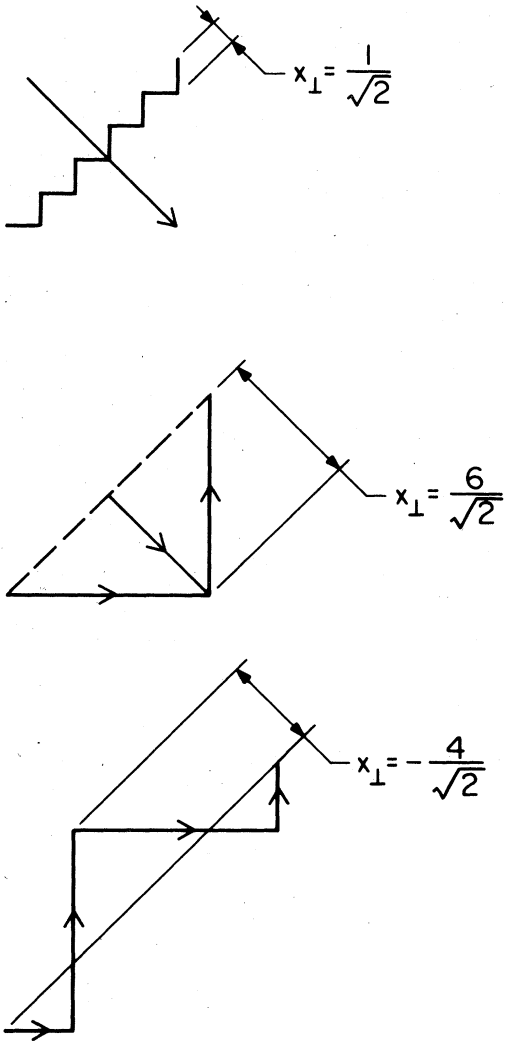

FIG. 5. Some typical 45° string states and their $x_\perp$ coordinate at the center.

were computed using the methods of Ref. 8. Since the string wave function involves a certain linear combination of the zeroth-order states discussed earlier, the "lattice constants" for the graphs shown in Fig. 7 involve computing such operators as "the average number of corners" in the string wave function. This is quite tedious.

To third order in x_s there are fourteen district graphs which are displayed in Fig. 7. Again the lattice constants for such graphs involve complicated matrix elements in the string wave function. In addition to these fourteen graphs there is a "Feynman graph" which involves a sum over excited intermediate string states and comes from a term of the form

$$\sum_{n\neq 0} |\langle 0|V(E_0 - H_0)^{-1} V|n\rangle|^2/(E_0 - E_n)$$

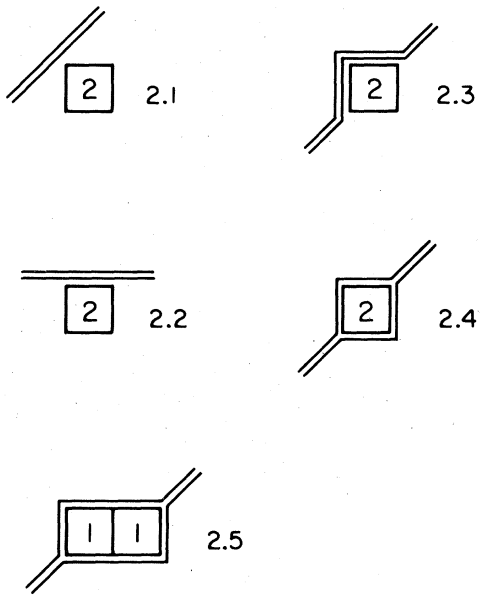

FIG. 6. The five second-order graphs projected into the plane. The numbers represent the number of times the potential acted.

familiar in ordinary Rayleigh-Schrödinger perturbation theory. Naively, such a term would be of fourth order in x_s, but since $E_0 - E_n$ is of order x_s, the total result contributes in third order.[9]

We have computed the second- and third-order corrections, $V_2(n_x, n_y)$ and $V_3(n_x, n_y)$. We have tabulated these values for various small values

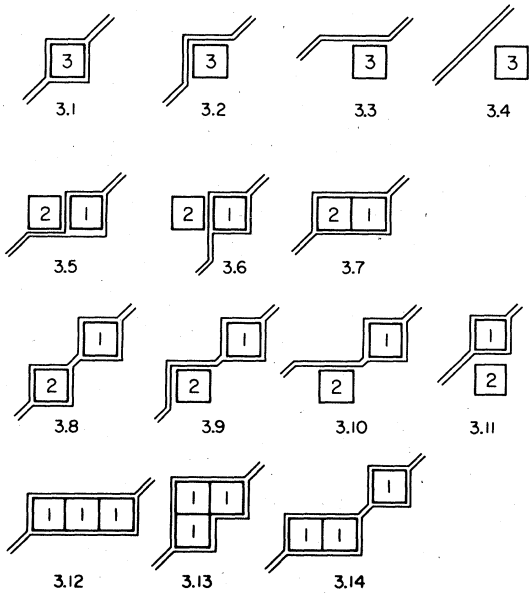

FIG. 7. The 14 third-order graphs. The lattice constants for these graphs involve complicated matrix elements in the string wave function.

of (n_x, n_y) in Table I. Using these results we may compute the string tension at 45°, that is,

$$T_{45^\circ} = \lim_{x\to\infty} \frac{V(x,x)}{\sqrt{2}x} \tag{2.16}$$

and compare how renormalizing the theory, holding the 45° tension fixed, differs from the on-axes case. To third order in x_s we find that

$$T_{45^\circ} = 1.8856 - 0.3001\,x_s - 0.2005\,x_s^2 - 0.0317\,x_s^3. \tag{2.17}$$

Notice that this series has a term linear in x_s in contrast to the 0° tension where such a term is not present.[1] By demanding that T_{45° is independent of the lattice spacing a, one induces a cutoff dependence in the bare coupling g_0 which is expressed in terms of the β function $(\beta_{45^\circ}(g_0))/g_0 = -d\ln g_0/d\ln a$. From the 45° tension series we find the third-order β function

$$\frac{-\beta_{45}(g_0)}{g_0} = 1 - 0.32\,x_s - 0.37\,x_s^2 + 0.12\,x_s^3. \tag{2.18}$$

Again, the major difference between the 45° series and the 0° one is the presence of the linear term in x_s in the 45° case. As expected this linear term flattens out the steep crossover region seen in the on-axes calculations.

If we examine the radial dependence of the $q\bar{q}$ potential at 45°, we find that to second order in x_s and to first order in $1/r$ that

$$V(r) = \frac{g_0^2}{2a}[(1.8856 - 0.3001\,x_s - 0.2005\,x_s^2)(r/a) + (0.12211\,x_s + 0.0652\,x_s^2) + (-0.0617\,x_s - 0.0285\,x_s^2)(a/r)]. \tag{2.19}$$

Note that the Coulomb term (the coefficient of $1/r$) is attractive, as one might expect from a weak-coupling analysis.

We now return to the general case $z \neq 0$, and the problem of computing the first-order correction to $V(x,y,z)$, namely, $V_1(n_x,n_y,n_z)$. This is a highly nontrivial problem to solve since for each point (n_x,n_y,n_z) one must diagonalize a matrix in a vector space of dimension $(|n_x|+|n_y|+|n_z|)!/|n_x|!|n_y|!|n_z|!$. For example, to compute $V_1(4,4,4)$ this involves $12!/(4!)^3 = 34\,650$ states, which is a nontrivial numerical problem.

We have been able to diagonalize the first-order mixing matrix for several small values of $r^2 = n_x^2 + n_y^2 + n_z^2$ and have listed some of these in Table II.

To see the approach to rotational invariance in the general case we plot our first-order results $V_0(n_x,n_y,n_z) + x_s V_1(n_x,n_y,n_z)$ against $r^2 = n_x^2 + n_y^2 + n_z^2$ and look for scattering at given r values.

TABLE I. Second- and third-order corrections to $V(x,y)$ for several values of (n_x,n_y).

(n_x,n_y)	$\frac{V_2(n_x,n_y)}{(n_x^2+n_y^2)^{1/2}}$	$\frac{V_3(n_x,n_y)}{(n_x^2+n_y^2)^{1/2}}$
(1,1)	−0.1633	−0.0181
(2,1)	−0.1595	−0.0206
(2,2)	−0.1802	−0.0156
(3,1)	−0.1461	−0.0256
(3,2)	−0.1778	−0.0172
(3,3)	−0.1865	−0.0150
(4,1)	−0.1347	−0.0291
(4,2)	−0.1694	−0.0205
(4,3)	−0.1851	−0.0159
(4,4)	−0.1898	−0.0146
(5,1)	−0.1258	−0.0314
(5,2)	−0.1603	−0.0237
(5,3)	−0.1797	−0.0181
(5,4)	−0.1889	−0.0153
(5,5)	−0.1918	−0.0145
(6,1)	−0.1189	−0.0329
(6,2)	−0.1520	−0.0263
(6,3)	−0.1730	−0.0206
(6,4)	−0.1851	−0.0168
(6,5)	−0.1912	−0.0149
(6,6)	−0.1932	−0.0143
(7,1)	−0.1135	−0.0339
(7,2)	−0.1447	−0.0283
(7,3)	−0.1663	−0.0229
(7,4)	−0.1802	−0.0187
(7,5)	−0.1885	−0.0160
(7,6)	−0.1927	−0.0147
(7,7)	−0.1942	−0.0142
(8,1)	−0.1091	−0.0346
(8,2)	−0.1384	−0.0299
(8,3)	−0.1599	−0.0249
(8,4)	−0.1749	−0.0206
(8,5)	−0.1847	−0.0175
(8,6)	−0.1907	−0.0155
(8,7)	−0.1939	−0.0145
(8,8)	−0.1950	−0.0142
(9,1)	−0.1055	−0.0351
(9,2)	−0.1330	−0.0311
(9,3)	−0.1541	−0.0266
(9,4)	−0.1696	−0.0224
(9,5)	−0.1805	−0.0191
(9,6)	−0.1887	−0.0167
(9,7)	−0.1923	−0.0152
(9,8)	−0.1947	−0.0144
(9,9)	−0.1956	−0.0141
(10,1)	−0.1026	−0.0354
(10,2)	−0.1283	−0.0320
(10,3)	−0.1488	−0.0280
(10,4)	−0.1645	−0.0241
(10,5)	−0.1760	−0.0207
(10,6)	−0.1843	−0.0180
(10,7)	−0.1899	−0.0162
(10,8)	−0.1934	−0.0149
(10,9)	−0.1953	−0.0143
(10,10)	−0.1961	−0.0141

For example, if the potential is rotationally invariant, we would expect the potential at (1, 1, 5) to be the same as the potential at (3, 3, 3). In Fig. 8 we have plotted our first-order result for various values of x_s. We see that for $x_s \simeq 2.3$ there is very little scatter in the data signaling a rotationally invariant potential.

These calculations summarize our results to this date. It is clear that this program is far from exhausted. Higher-order calculations are feasible and should be interesting. It will be particularly interesting to calculate more terms in the strong-coupling expansions of the functions $f_l(\theta, x_s)$ and obtain better numerical estimates of the power corrections r^{-l} to the confining potential. This will allow us to check string theory arguments for the universality of the r^{-1} term[5] and perhaps do some heavy-quark phenomenology from first principles.

TABLE II. First-order energy $V_1(n_x, n_y, n_z)$ for various small values of $r^2 = n_x^2 + n_y^2 + n_z^2$.

r^2	(n_x, n_y, n_z)	$V_1(n_x, n_y, n_z)$
0	(0,0,0)	0.0000
1	(0,0,1)	0.0000
2	(0,1,1)	−0.3333
3	(1,1,1)	−0.6667
4	(0,0,2)	0.0000
5	(0,1,2)	−0.4714
6	(1,1,2)	−0.8727
8	(0,2,2)	−0.7454
9	(0,0,3)	0.0000
9	(1,2,2)	−1.1519
10	(0,1,3)	−0.5393
11	(1,1,3)	−0.9965
12	(2,2,2)	−1.4597
13	(0,2,3)	−0.9107
14	(1,2,3)	−1.3437
16	(0,0,4)	0.0000
17	(0,1,4)	−0.5774
17	(2,2,3)	−1.6906
18	(0,3,3)	−1.1647
18	(1,1,4)	−1.0763
19	(1,3,3)	−1.5997
20	(0,2,4)	−1.0163
21	(1,2,4)	−1.4777
22	(2,3,3)	−1.9633
24	(2,2,4)	−1.8628
25	(0,0,5)	0.0000
25	(0,3,4)	−1.3424
26	(0,1,5)	−0.6006
26	(1,3,4)	−1.7909
27	(1,1,5)	−1.1306
27	(3,3,3)	−2.2596
29	(0,2,5)	−1.0873
29	(2,3,4)	−2.1760
30	(1,2,5)	−1.5746
32	(0,4,4)	−1.5863
33	(1,4,4)	−2.0351
33	(2,2,5)	−1.9933
34	(0,3,5)	−1.4705
34	(3,3,4)	−2.4964
35	(1,3,5)	−1.9357
36	(0,0,6)	0.0000
36	(2,4,4)	−2.4171
37	(0,1,6)	−0.6159
38	(1,1,6)	−1.1693
38	(2,3,5)	−2.3366
40	(0,2,6)	−1.1372
41	(0,4,5)	−1.7713
41	(1,2,6)	−1.6467

III. KINKS, ROUGHENING, AND THE RESTORATION OF ROTATIONAL INVARIANCE

Roughening and the restoration of rotational symmetry are intimately related phenomena. The bridge between them is provided by the "kink" mass, a quantity to be discussed here in some detail. First consider roughening. Place a static quark and an antiquark along an axis of a spatial lattice and let them be a distance N lattice spacings apart. In the strong-coupling limit ($x_s = 0$), a straight and static flux tube will form between them. At finite but small x the magnetic field term of the lattice Hamiltonian will cause the tube

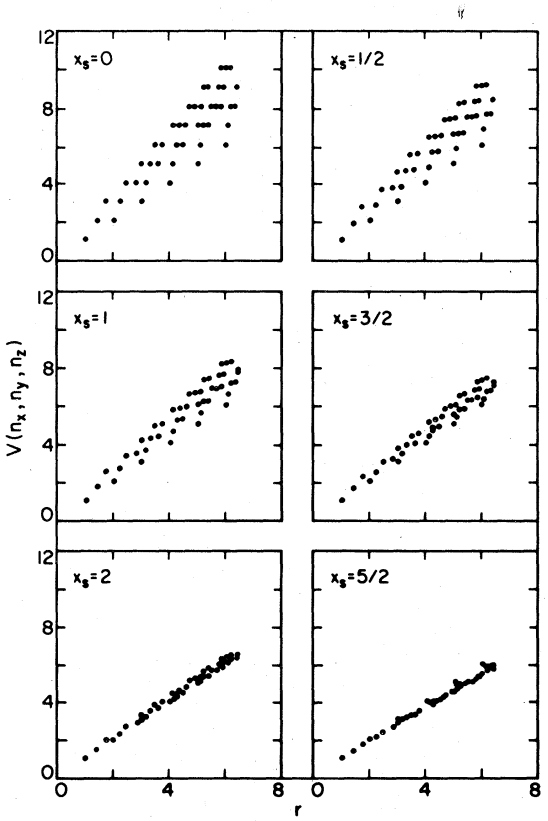

FIG. 8. $V_0(n_x, n_y, n_z) + x_s V_1(n_x, n_y, n_z)$ vs r^2. The scatter in the points is a measure of the rotational invariance.

FIG. 9. The lowest-order, lowest-energy fluctuation of a straight flux tube.

to fluctuate and thicken. The lowest-energy excitations consist of configurations of length $N+2$ with the flux in the fundamental representation. The zeroth-order energy of the configuration shown in Fig. 9 is $(g^2/2a)(4/3)(N+2)$, if the gauge group is SU(3). The fact that the energy of this configuration is a finite, nonzero amount above that of the straight tube implies that at sufficiently strong coupling these fluctuations will be sufficiently suppressed that the transverse extent (thickness) of the infinitely long string will be finite. The convergence of the strong-coupling expansion for small x_s means that there is a "smooth" phase for such flux tubes.

The lowest-energy, simplest-transverse excitation of the straight string is shown in Fig. 10—two arbitrarily long straight sections of string are connected by a single "kink." This configuration of flux has an energy $(g^2/2a)(\frac{4}{3})(N+1)$ in the strong-coupling limit—the transverse link costs $2g^2/3a$ units of energy. The existence of this mass gap in the spectrum of transverse excitations of the string implies that the transverse spatial distribution of the string is bounded. Now consider increasing x_s. Then fluctuations in the string occur and the mass gap decreases. There is the possibility that the kink mass vanishes at a finite value of $x_s = x_R$. At that point transverse excursions of an infinitely long string are no longer suppressed by an energy barrier so the string's mean width is expected to diverge. This is the character of the roughening transition. Our description here could apply to a quantum Hamiltonian analysis of the famous roughening of the interface in the three-dimensional Ising model.[10]

It is conventional to calculate the width of the string in strong-coupling expansions to search for the roughening transition x_R. Such calculations will be presented later in this article. However, we can also determine x_R by computing the kink mass and noting where it vanishes. Since this is a different approach to an old problem, we will relate it to more familiar descriptions of roughening before continuing. We can view the kink of Fig. 10 as an ordinary particle excitation living on the string. Let n denote its location in Fig. 10.

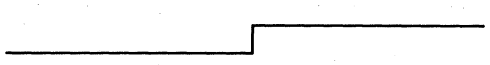

FIG. 10. The kink at strong coupling.

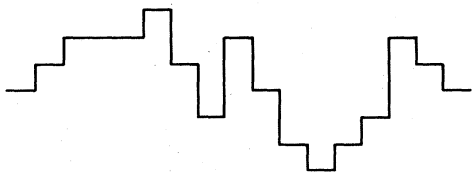

FIG. 11. The graphs included in the SOS approximation.

Then a kink of momentum $2\pi k/(N+2)$ is described by the state,

$$|k\rangle = \left(\frac{2}{N+2}\right)^{1/2} \sum_{n=0}^{N} \sin\left(\frac{2\pi k(n+1)}{N+2}\right) |n\rangle, \tag{3.1}$$

where N is the length of the straight string and k can be $1, 2, \ldots, N+1$. We will be particularly interested in kinks with $k=1$ since then their energy is a mass gap. In fact, in those cases in which roughening is well approximated by a solid-on-solid (SOS) model,[11] the kink is precisely the lowest-energy excitation of the $(1+1)$-dimensional field theory describing the wandering of the string. Consider the three-dimensional Ising model as an illustration. In the quantum Hamiltonian formulation the fluctuations of the interface are described by the $(1+1)$-dimensional Hamiltonian[4]

$$H = \sum_i |L_i - L_{i+1}| - x_s \sum_i \cos\phi_i, \tag{3.2}$$

where i labels a one-dimensional spatial lattice, and L_i is an operator on links which is canonically conjugate to ϕ_i,

$$[L_i, e^{\pm i\phi_i}] = \pm e^{\pm i\phi_i}. \tag{3.3}$$

Some thought reveals that Eq. (3.2) describes the graphs of the string illustrated in Fig. 11—a string fluctuates without "overhangs" in an inert background and L_i is the transverse position of the string on link i. This is the SOS model of the three-dimensional Ising model and it is thought to be a good approximation to the dynamics of the real interface for all temperatures near or below T_R, the roughening temperature. This is so because T_R is much less than the bulk critical point T_B so bulk fluctuations and overhangs are rare. Now consider Eq. (3.2) for x_s near zero. The lowest-energy state has all the L_i equal. Choose

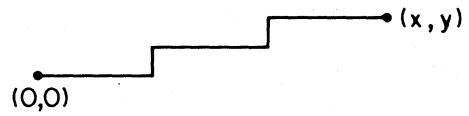

FIG. 12. A shortest path between a quark and an antiquark which contains two kinks.

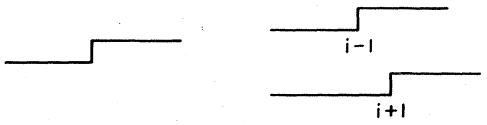

FIG. 13. (a) An initial kink at link i along a string. (b) Final-kink states after one application of the magnetic-field perturbation.

$L_i = 0$. This configuration describes the fixed string and the choice $L_i = 0$ has spontaneously broken the discrete translational symmetry in Eq. (3.2). The first excited state of the model, therefore, will have a single kink—L_i will be zero to the right (left) of a link j and will be one to the left (right) of link j. The second term in Eq. (3.2) allows the kink to propagate along the string and it also puts kink-antikink fluctuations on the string.

Now we turn to the connection between the kink and the restoration of rotational symmetry. We are particularly interested in the interquark potential. Place a quark at the origin and the antiquark at the lattice site (x,y,z). In a sensible, renormalized continuum limit of the theory, the static potential energy $V(x,y,z)$ should be spherically symmetric. However, in the strong-coupling limit it is clear that

$$V(x,y,z) = \frac{g^2}{2a}\frac{4}{3}(|x|+|y|+|z|) \tag{3.4}$$

since the flux must travel a path of minimal length from (0, 0, 0) to (x,y,z). For purposes of illustration choose $z = 0$ and let $V(x,y,0) \equiv V(x,y)$. The violation of rotational symmetry is substantial in Eq. (3.4)—along a ray $x = y$ Eq. (3.4) is a factor of $\sqrt{2}$ larger than the physical distance between the source and sink of flux. The equipotential surfaces of Eq. (3.4) have been shown in Fig. 2. The coordinate axes are singled out by the cusps in the equipotential surfaces. It is important and interesting to realize that this nonanalyticity in the spatial character of $V(x,y,z)$ is a consequence of the nonzero value of the kink mass at strong

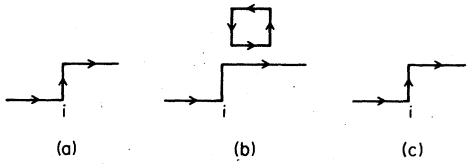

FIG. 14. Sequence of states in a contribution to second-order perturbation theory to the kink mass. The vacuum fluctuation is excluded from the string.

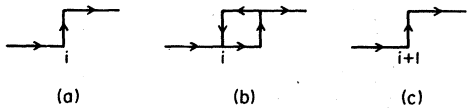

FIG. 15. As in Fig. 14, but the fluctuation lies on the kink which hops one site.

coupling. To see this consider $V(x,y)$ in the case that y is just a few lattice spacings while x is large and arbitrary. Then the configuration of flux is illustrated in Fig. 12—there are $|y|$ kinks on an otherwise straight string. Each $|y|$ kink costs an energy equal to m_k, the mass of the kink, so

$$V(x,y) = \frac{g^2}{2a}\frac{4}{3}|x| + m_k|y|. \tag{3.5}$$

If $a|x|$ is a macroscopic distance and $|y|$ is but a few links, then in a proper continuum limit having spherical symmetry only the first term in Eq. (3.5) should survive,

$$V(x,y) = TL, \tag{3.6}$$

where $L = ax$ and T is the celebrated string tension. So it is necessary that m_k vanish identically for the restoration of rotational symmetry. From our earlier discussion we expect m_k to be zero for all coupling g between g_R and the bulk critical point $g_B = 0$. So, at the roughening transition a source of the long-distance violation of rotational symmetry is eliminated. That leaves behind, of course, short-distance sources of rotational asymmetry such as lattice differences replacing continuous derivatives. These later effects should scale to zero at the bulk critical point as ordinary irrelevant operators.

Now we shall present results for the kink mass in a variety of lattice gauge theories. Consider a few illustrations taken from the SU(3) calculation in 3 + 1 dimensions. The method of calculation will be the strong-coupling expansion, and results to $O(g^{-16})$ will be obtained and analyzed. To zeroth order the energy of the kink Eq. (3.1) above the straight string is $\frac{4}{3}$ in units of $g^2/2a$ for SU(3). At first order in x_s the kink is able to

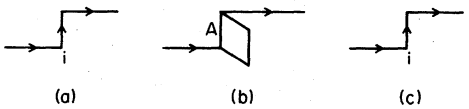

FIG. 16. As in Fig. 14, but the fluctuation lies out of the plane and a link on the string is excited to the representation A of SU(3).

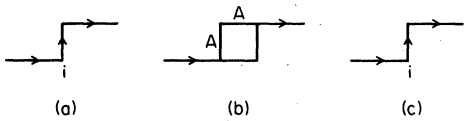

FIG. 17. As in Fig. 14, but the fluctuation lies on the kink and two links are excited to a flux representation A in the intermediate state.

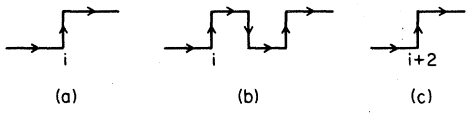

FIG. 18. As in Fig. 14 but the fluctuation lies on the string and permits the kink to hop two links to the left or right.

hop by one unit along the string as shown in Fig. 13. One must compute the matrix element of the magnetic field term $-x_s(\mathrm{tr}\,UUUU+\mathrm{H.c.})$ in the state Eq. (3.1). The result is $-2x_s/3$—the factor of 2 can be traced to the two directions along the string and the $\frac{1}{3}$ is an SU(3) group-theoretical weight. The second-order effects are more numerous and are shown in Figs. 14–18. These figures show the two intermediate states involved in the calculation of the matrix element of $V(E_0-H_0)^{-1}V$ familiar from ordinary Rayleigh-Schrödinger perturbation theory. In each case we compute the contribution to the intensive energy of the kink, i.e., a vacuum energy subtraction and a subtraction of the energy of the straight string is done order by order in x_s. The contributions from each graph are

$$(14)=\tfrac{3}{4}x_s^2\,, \tag{3.7a}$$

$$(15)=-\tfrac{1}{4}x_s^2\,, \tag{3.7b}$$

$$(16)=0\,, \tag{3.7c}$$

$$(17)=-2\sum_{A=3,6,8}\frac{\dim A}{9}\frac{1}{2C_A}x_s^2=-\frac{806}{1080}x_s^2\,, \tag{3.7d}$$

$$(18)=-\tfrac{1}{12}x_s^2\,. \tag{3.7e}$$

Besides the enumeration of graphs, the calculation requires the computation of lattice sums (e.g., in Fig. 14) one needs the number of ways a kink excludes a vacuum fluctuation) and SU(3) group theory [e.g., in Fig. 17 two links in the intermediate state are excited to representations $A=\bar{3}$, 6, or 8 each with a weight $\dim(A)/9$ and an energy denominator $(2C_A)^{-1}$, where C_A is the relevant quadratic Casimir operator]. These routine matters have been discussed at length elsewhere.[12] To continue to higher order it is helpful to have a table of SU(3) Racah coefficients[8] and to do the summations over intermediate states by computer. We will report the calculations of five terms in the strong-coupling series of the kink below. Since the calculations closely resemble those for the mass gaps in (1+1)-dimensional spin models, it should be possible to computerize the kink-mass calculation and obtain a series of ten to twelve terms. It should be worthwhile to pursue this because the results we will report below are quite interesting and are comparable in accuracy to the studies of roughening reported in the statistical mechanics literature.

In Tables III and IV we list the kink-mass series for Z_2, U(1), and SU(3) lattice gauge theories in 2+1 and 3+1 dimensions. The expansion parameters are defined through the following Hamiltonians. For Z_2 in 2+1 dimensions,

$$H=\frac{1}{2}\sum_{\text{links}}(1-\sigma_l)-x_s\sum_{\text{boxes}}\sigma_3\sigma_3\sigma_3\sigma_3\,. \tag{3.8}$$

Recall that this theory is dual to the Hamiltonian form of the three-dimensional Ising model.[12] The system's bulk critical point lies at $x_s=1.53\pm0.03$ (Ref. 13). For U(1) in 2+1 dimensions,

TABLE III. Strong-coupling series for the kink mass in (2+1)-dimensional lattice gauge theories. For SU(3) an overall factor of $\frac{4}{3}$ multiplies the series.

	ω_0	ω_1	ω_2	ω_3	ω_4
Z_2	1	−2	0	$\frac{1}{8}$	$\frac{1}{8}$
U(1)	1	−2	$\frac{1}{12}$	$\frac{25}{144}$	0.145 045 883
SU(3)	1	$-\frac{1}{2}$	−0.220 261 438	0.009 475 984	0.029 206 037

TABLE IV. Same as Table III except for (3+1)-dimensional theories.

	ω_0	ω_1	ω_2	ω_3	ω_4
Z_2	1	-2	$-\frac{1}{2}$	$\frac{5}{8}$	$-\frac{85}{96}$
U(1)	1	-2	$-\frac{1}{4}$	$\frac{35}{48}$	$-0.597\,554\,976$
SU(3)	1	$-\frac{1}{2}$	$-\frac{178}{720}$	$+0.006\,671\,073$	$0.031\,450\,710$

$$H \equiv \frac{g^2}{2} W = \frac{g^2}{2}\left(\sum_{\text{links}} L_l^2 - x_s \sum_{\text{boxes}} (\text{tr}\, UUUU + \text{H.c.}) \right), \tag{3.9}$$

where $x_s = 1/g^4 a^2$ is a dimensionless coupling constant in this superrenormalizable theory (g^2 has dimensions of mass). This system's bulk critical point lies at the origin $x_s^{-1} = 0$ where its correlation length diverges with an essential singularity.[14] The SU(3) theory in 2+1 dimensions has a similar form,

$$H \equiv \frac{g^2}{2} W = \frac{g^2}{2}\left(\sum_{l} E_l^2 - x_s \sum_{p} (\text{tr}\, UUUU + \text{H.c.}) \right), \tag{3.10}$$

where $x_s = 2/g^4 a^2$. The bulk critical point is thought to be at the origin $x_s^{-1} = 0$ and a nontrivial continuum limit which confines is expected. Now we turn to the theories in 3+1 dimensions. The Ising lattice gauge theory is described by Eq. (3.8), but in 3+1 dimensions its strong- and weak-coupling regions interchange under a duality map which has a self-dual coupling $x_s^* = \frac{1}{2}$ (Ref. 12). The strong-coupling phase confines and the theory undergoes a first-order phase transition[15] into a theory in which free charges exist at $x_s^* = \frac{1}{2}$. The U(1) theory in 3+1 dimensions has the Hamiltonian,

$$H \equiv \frac{g^2}{2a} W = \frac{g^2}{2a}\left(\sum L_l^2 - x_s \sum (\text{tr}\, UUUU + \text{H.c.}) \right), \tag{3.11}$$

where $x_s = 1/g^4$ and it also has two phases. The strong-coupling phase ($x_s \gtrsim 0.5$-0.6) confines electric charge and has a mass gap.[15] The weak-coupling phase admits free charge and contains a massless photon in its spectrum. The SU(3) theory in 3+1 dimensions was reviewed in the previous section. Numerical evidence is accumulating in support of the hypothesis that the theory has only one phase in which asymptotic freedom and confinement coexist.[1,2]

There are several ways of analyzing these series in search of zeros. We will discuss two methods. The first approach uses a strong-coupling series for the Callan-Symanzik β function of the kink mass. The kink mass is given by

$$m_k = \frac{g^2}{2a}\left(\sum_{n=0}^{\infty} \omega_n x_s^n \right), \tag{3.12}$$

where the coefficients ω_n are listed in Tables III and IV. The β function follows from the condition that m_k is a fixed physical quantity,

$$\frac{d}{da} m_k = 0 . \tag{3.13}$$

In order to satisfy Eq. (3.13), g must depend upon a in a specific fashion. Working out Eq. (3.13) by substituting into it Eq. (3.12), we find

$$-\beta(g)/g \equiv a \frac{\partial g}{\partial a} = \frac{\frac{1}{2}}{1 - 2x_s (W'/W)} , \tag{3.14}$$

where W is the dimensionless series in Eq. (3.12) for the kink mass. The β-function series are listed in Tables V and VI. The advantages in studying the β-function series are (1) its zeros label points x_c of second-order phase transitions; and (2) since it depends on the logarithmic derivative of W, it vanishes with a simple zero at x_c even if W itself vanishes with an anomalous dimension $W \sim (x_s - x_c)^{\nu}$. Our second approach will search for simple isolated poles in the series for $\ln^2 W$. The motivation for this comes from the three-dimensional Ising model in which the roughening transition is thought to be well approximated by the planar model in 1+1 dimensions. The strong-coupling end of this theory's critical line is described by the Kosterlitz renormalization group

TABLE V. Strong-coupling series for twice the β function of the kink mass in (2+1)-dimensional lattice gauge theories.

	β_0	β_1	β_2	β_3	β_4
Z_2	1	-4	8	$-\frac{61}{4}$	29
U(1)	1	-4	$\frac{25}{3}$	$-\frac{133}{8}$	33.021 478 17
SU(3)	1	-1	$-0.381\,045\,752$	$0.908\,163\,094$	$-0.016\,024\,113$

TABLE VI. Same as Table V except for (3+1)-dimensional theories.

	β_0	β_1	β_2	β_3	β_4
Z_2	1	−4	6	$-\frac{9}{4}$	$-\frac{289}{12}$
U(1)	1	−4	7	$-\frac{53}{8}$	−11.363 773 14
SU(3)	1	−1	$-\frac{22}{45}$	1.026 137 549	0.067 741 31

which predicts that as x_s approaches x_c from below, m_k should vanish with an essential singularity,[16]

$$\exp[-b/(x_c - x_s)^{1/2}] \tag{3.15}$$

whose $\ln^2$ is a simple pole.

Now consider the results of these analyses. The Padé tables for the β functions and $\ln^2 W$ are given in Tables VII–XVIII. We consider each case in turn.

(1) *Z_2 in 2+1 dimensions.* The Padé table for the β function indicates a stable zero at $x_R = 0.526$. However, this zero is accompanied by other zeros and poles at slightly larger values of x_s. This indicates that the β function has a cut on the real axis beginning at x_R and that m_k vanishes at x_R with a more complicated zero than $(x_c - x_s)^\nu$. The Padé Table VIII for $\ln^2 W$ is particularly satisfactory—there is good evidence for an isolated zero at $x_R = 0.576$. This gives some evidence for the Kosterlitz-Thouless description of the roughening transition.[16] Since $x_R = 0.576$ is much smaller than $x_B = 1.53 \pm 0.03$, we have good evidence for roughening deep inside the confining phase. This is the expected result.[10]

(2) *U(1) in 2+1 dimensions.* The analysis is very similar to the Z_2 theory in 2+1 dimensions. The Padé Table IX for the β function indicates a zero at $x_R = 0.549$, but this zero is accompanied by other singularities at slightly larger values of x_s. The hypothesis of Eq. (3.15) fits the series very well, however. The Padé Table X for the $\ln^2 W$ series shows good evidence for an isolated pole at $x_R = 0.601$. This is a particularly interesting result because x_B^{-1} is known to be precisely zero and the lattice theory is asymptotically free.[14]

(3) *SU(3) in 2+1 dimensions.* The qualitative features of this analysis are completely different from the Z_2 and U(1) Abelian theories. The Padé Table XI for the β function does not reveal a stable zero—as higher-order Padé approximants are constructed, the estimate of x_R moves toward weaker and weaker coupling g. It appears that $x_R \gtrsim 1.72$. The Padé table for $\ln^2 W$ does not reveal the presence of a simple pole and has not been included. The Padé Table XII for $\ln W$ is shown and gives some weak evidence for roughening at a relatively large value of $x_R \gtrsim 2.3$. We learn from all this that if the theory roughens, it does so only in the weak-coupling region $x_R \gtrsim 1.73$. In a later section width calculations will be discussed which also support this conclusion.

(4) *Z_2 in 3+1 dimensions.* The Padé analysis Table XIII for the β function indicates the presence of a cut beginning near the self-dual point $x^* = \frac{1}{2}$. The analysis of $\ln^2 W$ in Table SIV is clearer and shows good evidence for roughening at or slightly below the self-dual point. This gives some support for a Kosterlitz-Thouless description of roughening in this model. Note that our estimate of x_R does not differ greatly from that for the Z_2 model in 2+1 dimensions. We shall find that this trend is common to the groups studied, the roughening point is not strongly dimension dependent (while the bulk transition points are, of course).

(5) *U(1) in 3+1 dimensions.* Both the β function and $\ln^2 W$ Padé Tables XV and XVI show evidence

TABLE VII. Positions of the zero in the $[p,q]$ Padé approximants to the β function for Z_2 lattice gauge theory in 2+1 dimensions.

	1	2	3
1	0.500	0.525	0.526
2	0.527	0.526	
3	0.526		

TABLE VIII. Positions of the pole in the $[p,q]$ Padé approximant to the $\ln^2 W$ series for Z_2 lattice gauge theory in 2+1 dimensions.

	1	2	3	4
1	...	...	...	...
2	0.500	0.576	0.576	
3	0.565	0.576		
4	0.574			

TABLE IX. Same as Table VII except for U(1) gauge group.

	1	2	3
1	0.522	0.549	0.549
2	0.553	0.549	
3	0.549		

TABLE X. Same as Table VIII except for U(1) gauge group.

1	...	...	...	...
2	0.521	0.603	0.602	
3	0.591	0.602		
4	0.600			

for roughening at $x_R \simeq 0.56$. The analysis of the $\ln^2 W$ series is compatible with a Kosterlitz-Thouless transition. The bulk transition point has also been estimated to lie in the vicinity of 0.55, but the theoretical uncertainty in this number is large. It may be that $x_R = x_B$. This possibility deserves further attention.

(6) *SU(3) in 3+1 dimensions.* The analysis here is similar to that in 2+1 dimensions. The Padé Table XVII for the β function suggests that $x_R > 1.63$ and a higher-order calculation is necessary. The Padé Table XVIII for $\ln W$ does not reveal a definite transition but suggests $x_R \gtrsim 2.2$. The $\ln^2 W$ analysis is very erratic and several of the Padé approximants have no poles on the real axis. In a later section of this paper we shall see that calculations of the width of the string suggest that $x_R \simeq 1.80$. In summary, these calculations suggest that if the SU(3) theory roughens, it does so in the weak-coupling region. Recall from analyses of the string tension series that the theory has a strong-coupling region for $x_s \lesssim 0.40$, a crossover region for $0.40 \leq x_s \leq 1.44$, and a weak-coupling region for $x_s \gtrsim 1.44$ where ordinary perturbation theory applies.[1] Our roughening estimates lie well within this later region and suggest that roughening has nothing to do with the narrowness of the crossover region. In addition, the roughening transition does not constitute a barrier to the use of strong-coupling methods to describe the intermediate-coupling physics of the theory. This conclusion is different from that obtained in the Euclidean formulation of the SU(2) theory.[6] Series expansions for these models suggest that the string roughens in the crossover region. Since critical points are nonuniversal, these results do not contradict ours. If these estimates are accurate, then the Hamiltonian formulation of the model is a better framework for studying string dynamics and confinement. These points are worth pursuing. A final observation involves the use of SOS models for roughening in non-Abelian models. Since x_R lies in the weak-coupling region, the bulk systems are fluctuating wildly and the usual justifications for SOS approximations fail.

In summary, it is clear that the kink introduced here is a useful quantity both theoretically and computationally and that several of the ideas and calculations initiated here may be worth pursuing in greater depth.

TABLE XI. Same as Table VII except for SU(3) gauge group.

	1	2	3
1	0.712	1.611	...
2	0.894	1.720	
3	...		

TABLE XII. Same as Table VIII except for the lnW series of the SU(3) theory.

	1	2	3
1	1.423	...	...
2	2.417	2.293	
3	...		

IV. THE STRING WIDTH

At the roughening transition, fluctuations of the string with infinite amplitude have finite probability, leading to delocalization of the string. Thus, any reasonable definition of the string width will diverge at the transition point. We have therefore looked for this divergence as an alternative way of determining where (if at all) roughening does occur.

We choose only to consider those elements of the string and vacuum fluctuations parallel to the original direction of the string in our estimate, since these do give us a measure of the position of the string. Our density profile $\rho(x_\perp)$ at a distance $x_\perp$ from the string will be taken as the number of links, weighted by the square of the flux (eigenvalue of E^2) on the link, at $x_\perp$. The mean square string width is then given by

TABLE XIII. Same as Table VII except in 3+1 dimensions.

	1	2	3
1	0.400	0.548	...
2	...	0.467	
3	...		

TABLE XIV. Same as Table VIII except in 3+1 dimensions.

	1	2	3
1	0.400	···	0.455
2	0.543	0.499	
3	0.482		

$$\langle x_\perp^2 \rangle = \frac{\sum_{x_\perp} x_\perp^2 \rho(x_\perp)}{\sum_{x_\perp} \rho(x_\perp)} . \tag{4.1}$$

First let us consider the (2+1)-dimensional Ising model. Here the numerator in Eq. (4.1) is just

$$\left\langle \sum_{//\text{links}} x_\perp^2 \tfrac{1}{2}(1-\sigma_z) \right\rangle , \tag{4.2}$$

where the exception value is taken in the ground state of the Ising gauge theory with a string. To do this calculation, we use the Feynman-Hellman technique and evaluate the energy of a string state for the Hamiltonian,

$$H = \tfrac{1}{2} \sum_{\text{links}} (1-\sigma_z) + \frac{\lambda}{2} \sum_{//\text{links}} x_\perp^2 (1-\sigma_z) - x_s \sum_{\text{plaquettes}} \sigma_x \sigma_x \sigma_x \sigma_x \tag{4.3}$$

as a function of λ. If we call this energy E_λ,

$$\left\langle \sum_{//\text{links}} x_\perp^2 \tfrac{1}{2}(1-\sigma_z) \right\rangle = \frac{\partial E_\lambda}{\partial \lambda} \bigg|_{\lambda=0} . \tag{4.4}$$

We can now proceed to calculate E_λ as a perturbation series in x_s (high-temperature expansion for the Ising model). At zeroth order, E_λ is clearly n, independent of λ. To second order, E_λ (relative to the same quantity for the vacuum state) is given by the two graphs of Fig. 19. In Fig. 19(a) a vacuum fluctuation is created and subsequently annihilated on a plaquette not adjacent to the string. Such contributions are precisely canceled by the corresponding vacuum graph, which in addition subtracts contributions from adjacent the string giving

TABLE XV. Same as Table XIII except for U(1) gauge group.

	1	2	3
1	0.444	0.615	0.438
2	···	0.521	
3	···		

TABLE XVI. Same as Table XIV except for U(1) gauge group.

	1	2	3
1	0.444	···	0.505
2	0.608	0.556	
3	0.536		

$$\frac{2n}{4+\lambda} x_s^2 \tag{4.5a}$$

for Fig. 19(a).

In Fig. 19(b) one application of the perturbation on a plaquette adjacent the string produces a deformation of the string which is restored by a second application of the perturbation. This yields a contribution

$$\frac{-2n}{2+\lambda} x_s^2 . \tag{4.5b}$$

We have extended this calculation to sixth order for E_λ. After differentiation this yields

$$\langle x_\perp^2 \tfrac{1}{2}(1-\sigma_z) \rangle = n x_s^2 [\tfrac{3}{8} + \tfrac{29}{32} x_s^2 + \tfrac{1\,036\,423}{331\,776} x_s^4 + O(x_s^6)] \tag{4.6}$$

to sixth order.

A similar but much simpler calculation of $\langle \frac{1}{2} \sum_{//\text{links}} (1-\sigma_z) \rangle$ yields

$$\left\langle \frac{1}{2} \sum_{//\text{links}} (1-\sigma_z) \right\rangle = n[1 - \tfrac{1}{4} x_s^2 + O(x_s^6)] \tag{4.7}$$

to fourth order. The ratio to sixth order measured in units of the string tension T is then

$$T \frac{\langle \frac{1}{2} x_\perp^2 (1-\sigma_z) \rangle}{\langle \frac{1}{2}(1-\sigma_z) \rangle} = \tfrac{3}{8} x_s^2 [1 + \tfrac{13}{6} x_s^2 + \tfrac{871\,831}{124\,416} x_s^4 + O(x_s^6)] . \tag{4.8}$$

In order to analytically continue this series to the roughening point we write it as a [2,1] Padé approximant. This has a pole at

$$x_R = 0.556 , \tag{4.9}$$

where the width diverges, giving an estimate of the roughening point in good agreement with other

TABLE XVII. Same as Table XIII except for SU(3) gauge group.

	1	2	3
1	0.672	1.565	···
2	0.869	1.630	
3	···		

TABLE XVIII. Same as Table XII except in 3+1 dimensions.

	1	2	3
1	1.343	...	...
2	2.347	2.190	
3	...		

estimates.

Now we turn to the SU(3) gauge theory in 3+1 dimensions (lattice QCD). Here the numerator in Eq. (4.1) is

$$\left\langle \sum_{//\text{links}} x_\perp{}^2 \vec{E}^2 \right\rangle \tag{4.10}$$

while the denominator is

$$\left\langle \sum_{//\text{links}} \vec{E}^2 \right\rangle . \tag{4.11}$$

The quantity in Eq. (4.10) is calculated by the Feynman-Hellman theorem for the string state energy E_λ of the scaled Hamiltonian,

$$W = \sum_{\text{links}} \vec{E}^2 + \lambda \sum_{//\text{links}} x_\perp{}^2 \vec{E}^2 - x_s \sum_{\text{plaquettes}} \mathrm{Tr}[U_1 U_2 U_3 U_4 + \text{H.c.}] . \tag{4.12}$$

Perturbatively, to zeroth order in x_s, E_λ is $4n/3$ independent of λ. The second-order contribution is given by the graphs of Fig. 20. The only essential difference between these graphs and those of the Z_2 case is that (b) includes contributions where one link of the string is left in an excited state.

The contribution of Fig. 20(a) is

$$\frac{4n \times 2}{4 \times \frac{4}{3} + \frac{4}{3}\lambda} \tag{4.13a}$$

and that of Fig. 20(b)

$$\sum_A \frac{\dim(A)}{9} \frac{2n}{(2 \times \frac{4}{3} + C_A + \frac{4}{3}\lambda)} , \tag{4.13b}$$

where the sum runs over $A = 1, \bar{3}, 6$, and 8 and C_A is the quadratic Casimir operator for the representation A.

We have extended this calculation through fifth order in x_s with the result that

$$\left\langle \sum_{//\text{links}} x_\perp{}^2 E^2 \right\rangle = n(0.065\,845\,401\, x_s{}^2)[1 + 0.686\,227\,805\, x_s + 0.376\,072\,583\, x_s{}^2 + 0.230\,043\,416\, x_s{}^3 + O(x_s{}^4)] . \tag{4.14}$$

A similar calculation yields

$$\left\langle \sum_{//\text{links}} \vec{E}^2 \right\rangle = \tfrac{4}{3} n[1 - 0.044\,846\,534\, x_s{}^2 - 0.011\,711\,241\, x_s{}^2 - 0.004\,902\,915\, x_s{}^4 + O(x_s{}^5)] . \tag{4.15}$$

The string width in units of the string tension T is then

$$\frac{\langle \sum_{//\text{links}} x_\perp{}^2 \vec{E}^2 \rangle}{\langle \sum_{//\text{links}} \vec{E}^2 \rangle} \times T = (0.065\,845\,401\, x_s{}^2)[1 + 0.686\,227\,805\, x_s + 0.366\,997\,548\, x_s{}^2 + 0.207\,494\,028\, x_s{}^3 + O(x_s{}^4)] . \tag{4.16}$$

We have expressed the series as the [4, 1] and the [3, 2] Padé approximants. These have isolated poles at 1.7687 and 1.7879, respectively, so we predict to this order that the string roughens at

$$x_R = 1.77 - 1.79 . \tag{4.17}$$

However, examination of the ratios of successive coefficients of the series or of the Padé table indicates that the position of this pole has not yet

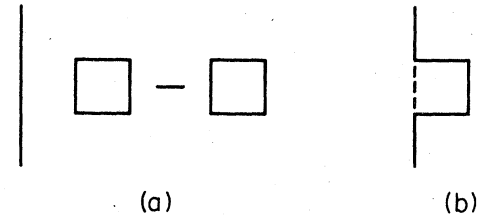

FIG. 19. (a) Vacuum fluctuation contributing to the width of the string in second order. (b) String fluctuation contributing to the width of the string.

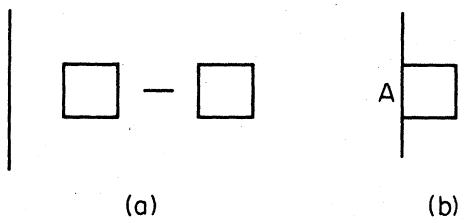

FIG. 20. (a) Vacuum fluctuation contributing to the width of the SU(3) string. (b) String fluctuation in second-order perturbation theory. A labels the SU(3) representation on the indicated link.

stabilized. The prediction is thus weakened to

$$x_R \gtrsim 1.77 . \tag{4.18}$$

This value of x_R lies in the weak-coupling domain of the theory $g \lesssim 1.03$ or $\alpha_s \lesssim 0.085$, in contrast with the Euclidean prediction,[6] and is not inconsistent with a roughening transition occurring at the bulk (zero-coupling) critical point, although it is suggestive of a roughening transition for a finite but small coupling.

ACKNOWLEDGMENTS

J.B.K., R.B.P., and J.L.R. acknowledge partial support from the National Science Foundation under Grants Nos. NSF-PHY79-00272 and NSF-PHY77-27084, respectively. J.S. acknowledges partial support by the U.S. Department of Energy under Grant No. DE-AC02-76ER03130. A 005 Task A-Theoretical.

[1]J. B. Kogut, R. B. Pearson, and J. Shigemitsu, Phys. Rev. Lett. 43, 484 (1979); Phys. Lett. 98B, 63 (1981); G. Munster, Nucl. Phys. B180, 23 (1981).

[2]M. Creutz, Phys. Rev. D 21, 2308 (1980).

[3]J. B. Kogut and L. Susskind, Phys. Rev. D 11, 395 (1975).

[4]G. Parisi, invited talk at the proceedings of the 1979 Cargese Summer School (unpublished); A. Hasenfratz, E. Hasenfratz, and P. Hasenfratz, Nucl. Phys. B180, 353 (1981); C. Itzykson, M. Peskin, and J.-B. Zuber, Phys. Lett. 95B, 259 (1980); M. Lüscher, G. Münster, and P. Weisz, Nucl. Phys. B180, 1 (1981).

[5]M. Lüscher, K. Symanzik, and P. Weisz, Nucl. Phys. B173, 365 (1980); M. Lüscher, Nucl. Phys. B180, 330 (1981); J. D. Stack and M. Stone, Illinois Report No. 80-51 1980 (unpublished).

[6]J. M. Drouffe and J. B. Zuber, Saclay Report No. DPh-T/80-128 (unpublished); G. Münster and P. Weisz, Nucl. Phys. B180, 13 (1981); DESY Report No. 80/97 (unpublished).

[7]R. B. Pearson and J. L. Richardson, ITP report, 1980 (unpublished).

[8]J. B. Kogut and R. Fredrickson, Illinois report, 1980 (unpublished).

[9]A. Carroll and J. B. Kogut, Phys. Rev. D 19, 2429 (1979).

[10]J. D. Weeks, G. H. Gilmer, and H. J. Leamy, Phys. Rev. Lett. 31, 549 (1973); S. T. Chui and J. D. Weeks, Phys. Rev. B 14, 4978 (1976).

[11]G. H. Gilmer and P. Bennema, J. Appl. Phys. 43, 1347 (1972).

[12]See, for example, J. B. Kogut, Rev. Mod. Phys. 51, 659 (1979).

[13]R. Elliot and P. Pfeuty, J. Phys. C 4, 2370 (1971).

[14]T. Banks, R. Myerson, and J. Kogut, Nucl. Phys. B129, 493 (1977), and references contained therein.

[15]J. Kogut, R. B. Pearson, J. Shigemitsu, and D. K. Sinclair, Phys. Rev. D 22, 2447 (1980).

[16]J. M. Kosterlitz, J. Phys. C 7, 1046 (1974).